The Effects of Impurities on Junction Behavior in High-Temperature Superconductors

Annual Report
Submitted to the Office of Naval Research
March 1, 2000

Principal Investigator: **Michael E. Flatté, Assistant Professor**
Department of Physics and Astronomy
University of Iowa, Iowa City, IA 52242
Phone number: **(319) 335-0201**
Fax number: **(319) 353-1115**
Email address: **michael-flatte@uiowa.edu**
Web site: **http://ostc.physics.uiowa.edu/~flatte**

20000403 027

Long term goals:

The project is a three-year effort focused on understanding and calculating the effects of impurities on the properties of high-temperature superconducting interfaces, particularly those of interest in tunneling devices. Building on theoretical tools developed during a previous ONR grant, which allow self-consistent, accurate calculations of the electronic properties near magnetic and nonmagnetic impurities at superconducting interfaces, various additional properties will be calculated. These include the effect of impurities or grain boundaries on supercurrent transport through a junction with arbitrary transparency and the effect of strong dynamic impurities on the nearby electronic structure. A particular emphasis will be placed on correlating theoretical calculations with experimental information.

Objectives:

To work with experimentalists to identify the signatures of particular impurities in junction performance.

To calculate the effect of impurities or grain boundaries on supercurrent transport through a junction with arbitrary transparency.

To calculate the effects of strong dynamic impurities on the nearby electronic structure, as well as junction behavior and other macroscopic properties such as the magnetic penetration depth.

To improve the bulk band structures used for high-temperature superconductors to those which reflect the best electronic structure models currently available.

To investigate defect and interface phenomena involving new materials.

Approach:

The influence of defects is calculated using a self-consistent Green's function approach (Koster-Slater technique) pioneered by the P.I. for impurity calculations in superconductors[1]. This technique will be generalized for planar junction applications and also for application to dynamic impurities. More detailed band structures will be obtained from multiband tight-binding parametrizations of full density-functional-theory calculations, as well as parametrizations of experimental probes of band structure such as angle-resolved photoemission.

Work completed:

The P.I. has performed detailed calculations of the properties of nickel and zinc impurities in the high-temperature superconductor $Bi_2Sr_2CaCu_2O_{8+\delta}$,(BSCCO) and compared with the recent observations of J. C. Davis at U. C. Berkeley. Scattering potentials for both nickel and zinc have been obtained by fitting the experiment. In the process the P.I. has demonstrated that the Zn atom locally destroys superconductivity in BSCCO. The P.I. has also suggested a method to probe the range of that local destruction of superconductivity through a two-impurity experiment. The P.I. has further proposed a sensitive method of probing the spin-spin correlation function in superconductors through an STM experiment involving two magnetic impurities.

Results:
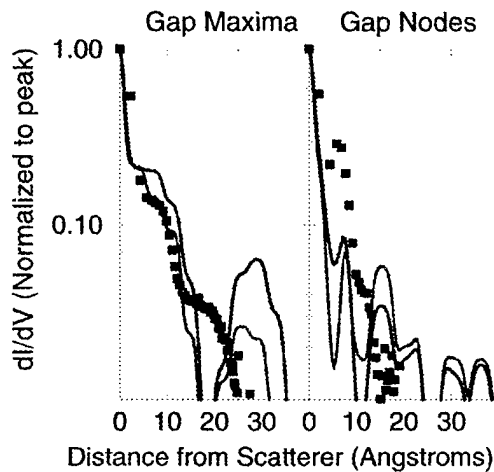*Local electronic structure of Zn and Ni impurities in $Bi_2Sr_2CaCu_2O_{8+\delta}$*

Recent observations by J. C. Davis near Zn and Ni impurities on a BSCCO surface indicate several surprising features of their local environment[2]. In particular, for Zn impurities the localized quasiparticle nearby appears to only have a hole-like component to it. Localized quasiparticle states, however, are expected to be roughly half electron and half hole. In addition, for both Zn and Ni two distinct localized states are seen by STM, although the second state near Zn is very weak. These two features, as well as two other minor discrepancies, required improvement of the theory of these localized states.

Zn impurities

The absence of the electron-like component to the localized quasparticle is explained if the Zn impurity locally disrupts the superconductivity. Near the Zn impurity it is possible that the phase coherence of the superconducting state has been disrupted[3]. Thus a localized state which is purely hole-like at the impurity will not mix with electron-like components through Andreev processes. An alternative possibility is that the Zn locally nucleates an alternate order parameter, such as an antiferromagnetic order parameter. In this case again Andreev processes will not exist. Good agreement has been obtained for the local spectrum by assuming that Andreev processes are absent or phase-incoherent, and also assuming that there is a small magnetic component to the Zn impurity. This small magnetic component produces an additional resonance at a separate energy, as shown below. Figure 1 shows a comparison of experimental results (black) with theoretical calculations for a system with an alternate order parameter near the impurity (blue) and a system without phase coherence (red). The agreement is quite good for both. Figure 2 shows the amplitude of the resonance near the impurity compared with experiment along two directions (gap maxima and gap nodes), and Figure 3 shows the amplitude of the resonance spatially around the impurity.

Impurity site

y-axis: dI/dV Junction normalized at -200mV

x-axis: Voltage (mV) — 30, 0, 30
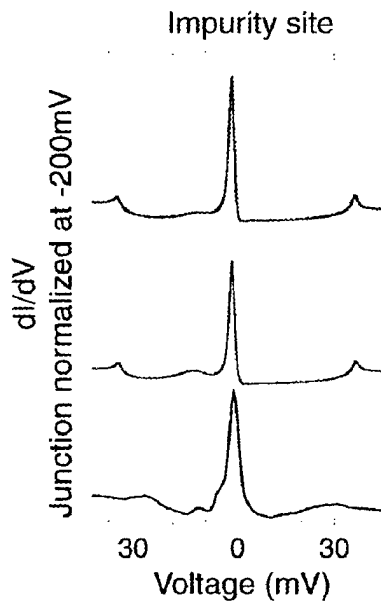
Fig. 1: Theoretical calcultions (blue, red) and experimental measurements (black) for the differential conductance (dI/dV) over a Zn atom near the surface of BSCCO. The blue curve is for an alternate order parameter in the vicinity of the impurity, the red curve is for phase-incoherent Andreév processes. The Zn atom is assumed to have a repulsive on-site potential for electrons of (blue, 0.543eV; red, 0.825 eV), and a magnetic component of (blue 0.29eV, red 0.55eV). The large amplitude of the resonance on this site and the presence of gap features are well reproduced by the theory.

Gap Maxima   Gap Nodes

y-axis: dI/dV (Normalized to peak) — 1.00, 0.10

x-axis: Distance from Scatterer (Angstroms) — 0 10 20 30 0 10 20 30

Fig. 2: Results for the above calculations near the impurity. The agreement is excellent along the directions of the gap maxima, and acceptable along the directions of the gap nodes.

40, 20, 0, -20, -40

-40 -20 0 20 40

1
0.1
0.01
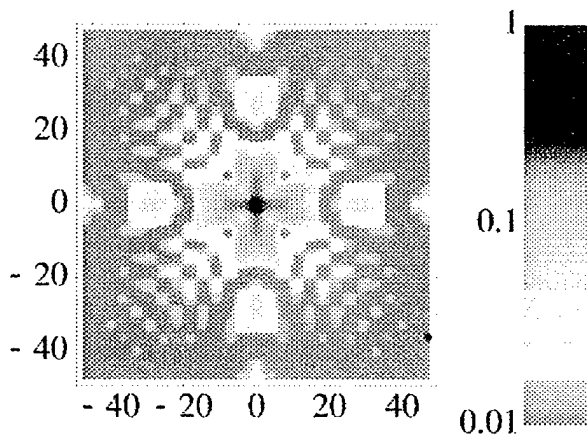
Fig. 3: Calculated plot of differential conductance at the energy of the resonance (-1.5mV). The direction of the gap maxima is horizontal.

The excellent agreement between theory and experiment has been achieved through use of an empirical electronic structure obtained from angle-resolved photoemission data[4]. Recently this empirical parametrization of the BSCCO electronic structure has been improved in the light of further photoemission and neutron scattering data[5]. It is possible that these changes will improve the agreement between theory and experiment. This is currently under investigation.

Ni impurities

For nickel impurities the two resonances are more resolvable. As shown below in Figure 4 they are both on the electron-like side of the spectrum on the Ni atom. In contrast to the case with Zn, here the resonance is seen on both the hole and electron like side of the spectrum. Thus the Ni atom does not disrupt superconductivity in the way the Zn atom does. The Ni atom potential is also much weaker: -0.305eV for the nonmagnetic component, and 0.115eV for the magnetic component. This may explain why the local superconductivity is not destroyed.
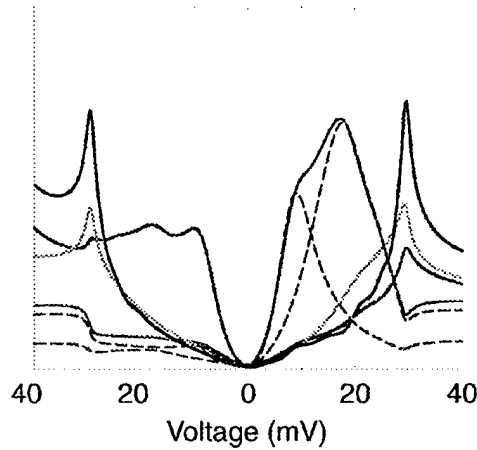
Fig. 4: . The red curve shows the on-site spectrum the blue curve shows the nearest-neighbor one, and the green curve shows the next nearest-neighbor spectrum. The black curve shows the spectrum far from the impurity. The two peaks correspond to one spin up and one spin down resonant state. These two states are resolved in the on-site spectrum with the two red dashed lines.
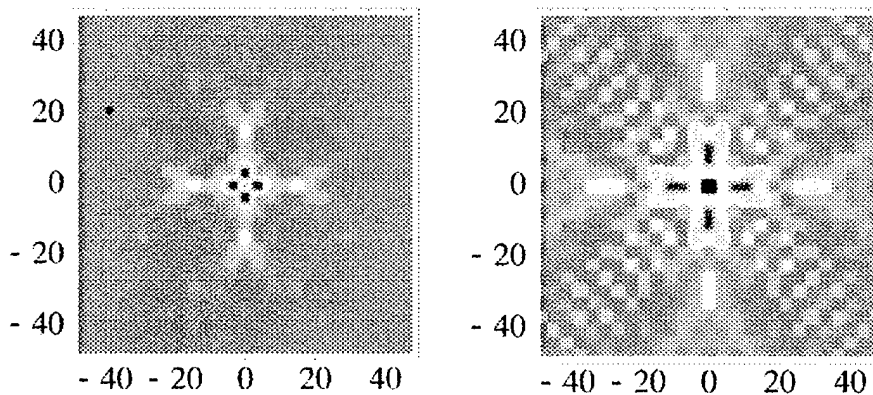
Fig. 5: On the left is a slice at a sample voltage of –9mV, whereas on the right the voltage is 9mV. These two slices show the hole-like and electron-like components of the resonant state at that energy. The hole-like component vanishes along the diagonals (along the gap nodes), as seen in the experiment.

As seen in Figure 5 the spatial structure of the electron and hole like components of the quasiparticle resonances are quite different. This occurs because of the *d*-wave order parameter of the superconductor.

Use of Ni and Zn impurities to probe local superconductivity

The effect of the Ni and Zn impurities can be used to probe the local superconducting properties of BSCCO. By placing a Ni atom near the Zn atom and examining whether both an electron and hole-like component are visible in the spectrum, the range of the destruction of superconductivity can be probed. Also, by examining the spectrum of two Ni atoms it can be determined whether the Ni moments are parallel or antiparallel – thus probing directly the spin-spin correlation function[6].

Impact/Applications:

An improved understanding of single-impurity properties will allow for an improved understanding of macroscopic quantities which depend on many impurities. These include, in addition to junction performance, the magnetic penetration depth and dielectric loss, which are important for superconductor-based mixers. Experiments involving more than one impurity, such as the two-impurity experiment proposed by the P.I., will allow experimentalists to extract local information about the superconducting state, and perhaps to disentangle the extrinsic inhomogeneity of the state from any intrinsic inhomogeneous character.

Transitions:

None

Related Projects:

The experimental program of J. C. Davis at UC Berkeley is the most closely related project. Other projects involved in the understanding and characterization of junction behavior, such as that of R. Buhrman at Cornell are also related. Projects involved in understanding the origin of dielectric loss, such as S. Sridhar's at Northeastern, are expected to become more related over the next year.

References:

1) M. E. Flatté and J. M. Byers, in *Solid State Physics Vol. 52*, pp. 137-228 (1999).
2) S. H. Pan, *et al.*, Nature **403**, 746 (2000).
3) e.g. V. J. Emery and S. A. Kivelson, Nature **374**, 434 (1995).
4) M. R. Norman, M. Randeria, H. Ding, and J. C. Campuzano, Physical Review B **52**, 615 (1995).
5) M. R. Norman, preprint.
6) M. E. Flatté and D. E. Reynolds, *Physical Review B in press.*

Publications:

Refereed Publications (attached):

1) "The local spectrum of a superconductor as a probe of interactions between magnetic impurities", Michael E. Flatté and David E. Reynolds, *Physical Review B in press*.

2) "Quasiparticle resonant states as a probe of short-range electronic structure and Andreév coherence", Michael E. Flatté, submitted to *Physical Review Letters*.

Invited Talk:

1) "Quasiparticle resonant states near defects near the BSCCO surface", March Meeting of the American Physical Society, Minneapolis, MN, March 20, 2000.

Selected Contributed Poster:

1) "Quasiparticle resonant states in $Bi_2Sr_2CaCu_2O_{8+\delta}$", 6th International Conference on Materials and Mechanisms of Superconductivity and High-Temperature Superconductors, Houston, TX, February 22, 2000.

Patents:

None.

Quasiparticle resonant states as a probe of short-range electronic structure and Andreév coherence

Michael E. Flatté

Department of Physics and Astronomy, University of Iowa, Iowa City, IA 52242

Abstract

The recently observed properties of quasiparticle resonant states near impurities on the surface of superconducting $Bi_2Sr_2CaCu_2O_{8+\delta}$ demonstrate that in-plane Andreév processes are either absent or phase-incoherent. Analysis of the spectral and spatial details of the electronic structure near a Zn impurity also suggest an effective magnetic component of the impurity potential. Further experiments are proposed to clarify whether the effective moments of nearby impurities are correlated.

Over the past few years several authors have emphasized the wealth of information available from local probes of impurity properties in correlated electron systems, and particularly in superconductors whose homogeneous order parameters (OP) are anisotropic in momentum [1]. A parallel improvement in scanning tunneling spectroscopy (STS) has allowed this vision to become a reality through direct observation of the local density of states (LDOS), first in niobium [2], which has a momentum-independent OP, and this year in the high-temperature superconductor $Bi_2Sr_2CaCu_2O_{8+\delta}$ (BSCCO) [3–5], which has an anisotropic OP. The electronic structure of the BSCCO surface is much more complex than that of the niobium surface; there are local moments in the copper-oxygen planes and, under certain conditions, a pseudogap state. Recent work [6] has emphasized the role of the pseudogap state [7–9] in determining the properties of clean surfaces of high-temperature superconductors at temperatures near T_c, and STS and photoemission have directly demonstrated its existence on the surface of BSCCO. The pseudogap state is characterized by a single-particle gap of $d_{x^2-y^2}$ symmetry, but the Andreév processes one would expect in a superconducting state are (according to differences in mechanism) either absent or phase-incoherent.

Here the STS measurements near impurities [3–5] will be shown to unambiguously demonstrate essentially complete suppression of Andreév processes in the vicinity of the impurity, even at very low temperatures. This low-temperature indication of a pseudogap implies its importance to the nature of the superconducting state and the operation of devices (such as Josephson junctions) with such materials. Indications of an effective magnetic component can also be seen in Ref. [5]. Thus STS provides a direct probe of both the local Andreév (superconducting) coherence and the local magnetic properties on the BSCCO surface.

A brief review of the experimental results from Refs. [3–5] is in order. Theoretical predictions which have been confirmed include the presence of quasiparticle resonances near nonmagnetic impurities in anisotropic OP superconductors [10], as well as the suppression of the gap feature near the impurity and the asymmetry of the resonance peak due to the energy dependence of the quasiparticle density of states [11]. The disagreements with previous theory, however, are striking. The most noticeable one is that the resonant state has only been detected on the *hole* side of the spectrum, both on the impurity site and *everywhere else around the impurity*. Whereas previous theories are consistent with an LDOS measured at the impurity which is entirely hole-like, these same theories unambiguously predict the LDOS at nearest-neighbor states will be almost entirely electron-like. Indeed these theories predict the spatially-integrated LDOS (or DOS) will be nearly particle-hole symmetric even though the LDOS at any particular site is not. A second unexpected element in the data is the presence of a second, much smaller, spectral peak on the hole side in Ref. [5]. Whereas previous theories are consistent with two resonances at a single impurity, the spatially-integrated amplitude of each resonance should be approximately the same, unlike what is seen in Ref. [5].

The above two issues are disagreements between the experimental and theoretical DOS, but there are also two significant disagreements in the LDOS. The resonance has a large amplitude at the impurity site, whereas calculations indicate that the largest amplitude in

the LDOS should occur at the nearest-neighbor sites. Finally, the gap feature is seen on the impurity site, where it does not appear in calculations. [1]

The calculations here incorporate the pseudogap state into the evaluation of the differential conductance (dI/dV). After evaluating the LDOS for several impurity potential models, allowing for spatial extent and magnetic character in the potential, the impurities of Refs [3–5] are found to be highly localized and the four discrepancies above can be reconciled. Finally, in the case of Ref. [5], a magnetic component to the effective Zn impurity potential is evident. [12]

The calculations of the LDOS are based on the Hamiltonian

$$ H = \sum_{\langle ij\rangle,\sigma} \left[-t_{ij}c_{i\sigma}^{\dagger}c_{j\sigma} + \Delta_{ij}c_{i\uparrow}^{\dagger}c_{j\downarrow}^{\dagger} + \Delta_{ij}^{*}c_{j\downarrow}c_{i\uparrow} \right] + \sum_{i} \left[(V_{0i} + V_{Si})c_{i\uparrow}^{\dagger}c_{i\uparrow} + (V_{0i} - V_{Si})c_{i\downarrow}^{\dagger}c_{i\downarrow} \right], \quad (1) $$

which includes a site-dependent potential which can be magnetic (V_S), nonmagnetic (V_0), or a combination of both. i and j label sites and σ labels spin. The homogeneous electronic structure, expressed as hopping matrix elements (t_{ij}) for the first five nearest neighbors, is taken from a single-band parametrization of photoemission data. [13] Large variations in hopping matrix elements (> 50 meV) produce results very much at odds with experiment, whereas smaller variations are mimicked by the site-dependent potential. Hence such changes will be ignored here. Only on-site and nearest-neighbor order parameters Δ_{ij} are nonzero, and the maximum OP on the Fermi surface, $\Delta_{max} = 40$ meV. [14]

The electronic structure of the inhomogeneous system (including the impurity) is determined by direct numerical solution in real space of the Gor'kov equation (in Nambu form) for the inhomogeneous Green's function, $\mathbf{G} = \mathbf{g} + \mathbf{g}\mathbf{V}\mathbf{G} = (\mathbf{I} - \mathbf{g}\mathbf{V})^{-1}\mathbf{g}$, within a real-space region around the impurity beyond which the potential is negligible. [1] The Δ_{ij}'s are found self-consistently in this process, for they determine the off-diagonal components of the potential $\mathbf{V}$. Spectra outside this real-space region are constructed according to the generalized T-matrix equation: $\mathbf{G} = \mathbf{g} + \mathbf{g}\mathbf{V}\left[\mathbf{I} - \mathbf{G}\mathbf{V}\right]^{-1}\mathbf{g}$. Once $\mathbf{G}$ has been calculated throughout the region near the impurity, the LDOS and DOS are obtained from its imaginary part and the lattice Wannier functions. Then

$$ \frac{dI(\mathbf{x};V)}{dV} = -\int d\omega \sum_{\sigma} \frac{1}{\pi} \left(\frac{\partial n_{STM}(\omega)}{\partial \omega} \right) |\phi_{\sigma}(\mathbf{x};i)|^2 \mathrm{Im}G_{\sigma}(i,i;\omega), \quad (2) $$

where $\phi_{\sigma}(\mathbf{x};i)$ is the overlap of the Wannier function at site i and spin σ with the STM tip at $\mathbf{x}$, and $n_{STM}(\omega)$ is the occupation function of the STM tip. [1] Resonances correspond to new peaks in the differential DOS (the difference between the inhomogeneous and homogeneous DOS); their energies are shown in Fig. 1(ab) for magnetic and nonmagnetic single-site impurities.

If Andreév processes are suppressed, either by reduction in their amplitude or phase coherence, a resonance's DOS will become more electron-like or more hole-like. Reduction of the amplitude of the homogeneous anomalous Green's function $f(i,j;\omega)$, due perhaps to a local antiferromagnetic (AF) order, decreases the mean-field coupling between electron and hole excitations. Note that this is very different from the fully electron or hole-like

character of the *LDOS* at the impurity, which originates from a vanishing $f(i,i;\omega)$ in the $d_{x^2-y^2}$ state. Figure 1(cd) shows the DOS of a resonance for three systems with a 40 meV $d_{x^2-y^2}$ gap: a fully superconducting gap (solid line), a gap with a 25 meV superconducting component (dashed line), and a pseudogap with no superconducting component (dot-dashed line). As the superconducting component is reduced, the electron-hole symmetry diminishes. The nonmagnetic potentials of Fig. 1(c) are chosen (1.375 eV, 1.000 eV, and 0.833 eV, respectively) so the resonance peak is at −1.5 mV (the same as Ref. [5]). The magnetic potentials in Fig. 1(d) are the same as those in Fig. 1(c).

The reduction of the electron-like peak from phase decoherence is similar to the effect of amplitude suppression of $f(i,i;\omega)$. For a resonance at ω, the peak at $-\omega$ comes from terms with products of pairs of anomalous Green's functions. For a phase incoherent pseudogap state the expectation value of these pairs, and thus the amplitude of the electron-like peak, is diminished. [8] The effect of this is shown in Fig. 1(ef) as a dashed line corresponding to partial (half) and a dot-dashed line corresponding to no phase coherence. The nonmagnetic potential is 1.375 eV in Fig. 1(e) and the magnetic potential is 1.375 eV in Fig. 1(f). Note that for the purely magnetic impurities even in the absence of Andreév coherence there is a peak on each side of zero energy.

For Refs. [3,5] there is no apparent electron-like component of the resonance in the DOS, thus local Andreév coherence is absent. In measurements of the LDOS near metal islands on BSCCO [4], however, both hole-like and electron-like peaks are apparent. This may indicate that the metal plays an important role in maintaining phase coherence at the surface, or that the metal overlayer is less disruptive to superconductivity than impurities in the plane. The presence of the in-plane Andreév processes, indicated by the electron-like peak, is essential to the operation of Josephson junctions.

The on-site LDOS of Ref. [5] is shown in Fig. 2(a). The second (hole-like) peak is not as clearly evident in the results of Refs. [3,4], and thus may be peculiar either to the Zn impurity or to the impurity site in the BSCCO unit cell. Additional resonances around impurities can originate from additional orbital states around spatially-extended potentials or from spin-splitting near magnetic potentials. Note that an effective magnetic potential could also originate from a nonmagnetic impurity potential placed in a spin-polarized host electronic structure.

Figure 2(abc) shows the best fit of dI/dV to the data of Ref. [5] for phase incoherent Andreév processes and *i* a single-site nonmagnetic potential (1.375 eV), *ii* a nonmagnetic potential with onsite (0.360 eV) and nearest-neighbor (0.150 eV) values, and *iii* a mixed nonmagnetic and magnetic potential ($V_0 = 0.825$ eV, $V_S = 0.550$ eV). Also shown is the best fit using *iv* a pseudogap with no superconducting component and a mixed potential ($V_0 = 0.543$ eV, $V_S = 0.290$ eV). The three panels show dI/dV (a) at the impurity site, (b) at the nearest-neighbor site along the gap nodes, and (c) along the gap maxima. Measurements of Ref. [5] for (a) and (b) are shown; (c) is not available.

The large size of the resonance on-site and the simultaneous presence of the gap feature occur because of junction normalization (equal resistance at −200 mV) and the finite width of the $|\phi_\sigma|^2$ (modeled as Gaussians of range 0.8Å, 3.8Å, 0.8Å, and 1.0Å for *i-iv*). The very

4

small LDOS in this energy range at the impurity site causes the tip to approach closer to the surface and (1) enlarge the apparent size of the resonance on-site, and (2) pick up the gap features from the nearest-neighbor sites. The relative size of the on-site resonance to the gap features is largely determined by the overlap of the nearest-neighbor Wannier functions with the tip when the tip is over the impurity site.

Judging from the comparison with experiment, *iii* and *iv* appear most in agreement. *i* does not have a second resonance, and whereas *ii* does show one in the proper location, its relative magnitude is incorrect. The smaller amplitude of the second resonance is obtained for *iii* and *iv* because the overlaps with the STM tip are spin-dependent ($|\phi_\uparrow(\mathbf{x})|^2/|\phi_\downarrow(\mathbf{x})|^2 \sim 40$). If the second peak were absent, either the impurity would lack magnetic character, or it would occur in less magnetic regions of the BSCCO unit cell. The remaining disagreement is in the amplitude of the resonance in (B), where *iv* is best, but still too small.

Figure 3 shows the amplitude of the resonance as a function of distance from the impurity along the gap maxima (a) and the gap nodes (b). The squares are the data from Ref. [5], whereas the solid line corresponds to *iii*, the dotted line to *ii*, and the dot-dashed line to *iv*. The plot for *i* looks identical to that of *iii*. The agreement of *iii* and *iv* are quite good along the maxima direction. The absence of a well-defined maximum at the nearest-neighbor in (a), which was pointed out in Ref. [5], is due to the normalization procedure. An inset in Fig. 3 shows the difference between the junction normalized (solid) and unnormalized (dashed) dI/dV. The main discrepancy is with the amplitude of the signal along the node directions (b).

Figure 4 shows the dI/dV of the resonance for *iv*; *iii* is similar. The differences between the Figs. 2-4 and the measurements of Ref. [5] may be due to errors in the homogeneous electronic structure of BSCCO used in the calculation, particularly the low-energy electronic structure which dominates the longer-range LDOS. These errors may be due to inaccuracies in the model for the electronic structure measured by photoemission [13], or they may be due to the neglect of other collective effects on the surface. Another likely source of error is that the electronic structure model of the host is not spin dependent.

One of the possible mechanisms of a pseudogap is local AF order, such as occurs in a stripe. [9] The magnetic component apparent in the impurity potential suggests this origin as well. If two nearby local moments are aligned parallel, then the resonances associated with them will hybridize and split [15], whereas if they are antiparallel the resonances will be degenerate. A careful examination of the dI/dV for two Zn atoms near each other on the surface may clarify whether there is local AF order.

The LDOS reported in Refs. [3–5] are best explained by the presence of a pseudogap state on the surface of BSCCO. The relative height of the electron-like and hole-like resonances in the DOS depends directly on the amplitude of local Andreév processes, and thus shows the degree of local superconducting coherence. This is of great practical interest, for the presence of these processes is essential to forming a proper Josephson junction across an interface. The information obtained about the superconducting state at the surface of BSCCO indicates the clear promise of future STM measurements near defects in other correlated electron systems.

REFERENCES

[1] See M. E. Flatté and J. M. Byers, in *Solid State Physics Vol. 52*, ed. H. Ehrenreich and F. Spaepen, (Academic Press, New York, 1999), and references therein.

[2] A. Yazdani, *et al.*, *Science* **275** 1767 (1997).

[3] E. W. Hudson, *et al.*, *Science* **285**, 88 (1999).

[4] A. Yazdani *et al.*, *Phys. Rev. Lett.* **83**, 176 (1999).

[5] S. H. Pan, *et al.*, *Nature (London)* in press (cond-mat/9909365).

[6] A. G. Loeser, *et al.*, *Science* **273**, 325 (1996); Ch. Renner, *et al.*, *Phys. Rev. Lett.* **80**, 149 (1998).

[7] G. V. M. Williams, *et al.*, *Phys. Rev. Lett.* **78**, 721 (1997); G. Deutscher, *Nature (London)* **397**, 410 (1999).

[8] L. B. Ioffe and A. J. Millis, *Science* **285**, 1241 (1999).

[9] V. J. Emery and S. A. Kivelson, *Nature (London)* **374**, 434 (1995).

[10] M. A. Salkola, A. V. Balatsky, and D. J. Scalapino, *Phys. Rev. Lett.* **77**, 1841 (1996).

[11] M. E. Flatté and J. M. Byers, *Phys. Rev. Lett.* **80**, 4546 (1998).

[12] This has been seen in YBCO (A. V. Mahajan, *et al.*, *Phys. Rev. Lett.* **72**, 3100 (1994)).

[13] M. R. Norman, M. Randeria, H. Ding, and J. C. Campuzano, *Phys. Rev. B* **52**, 615 (1995).

[14] Measured gap features at the surface vary from sample to sample as well as from point to point on the same sample. 40 meV is a typical location for the gap feature.

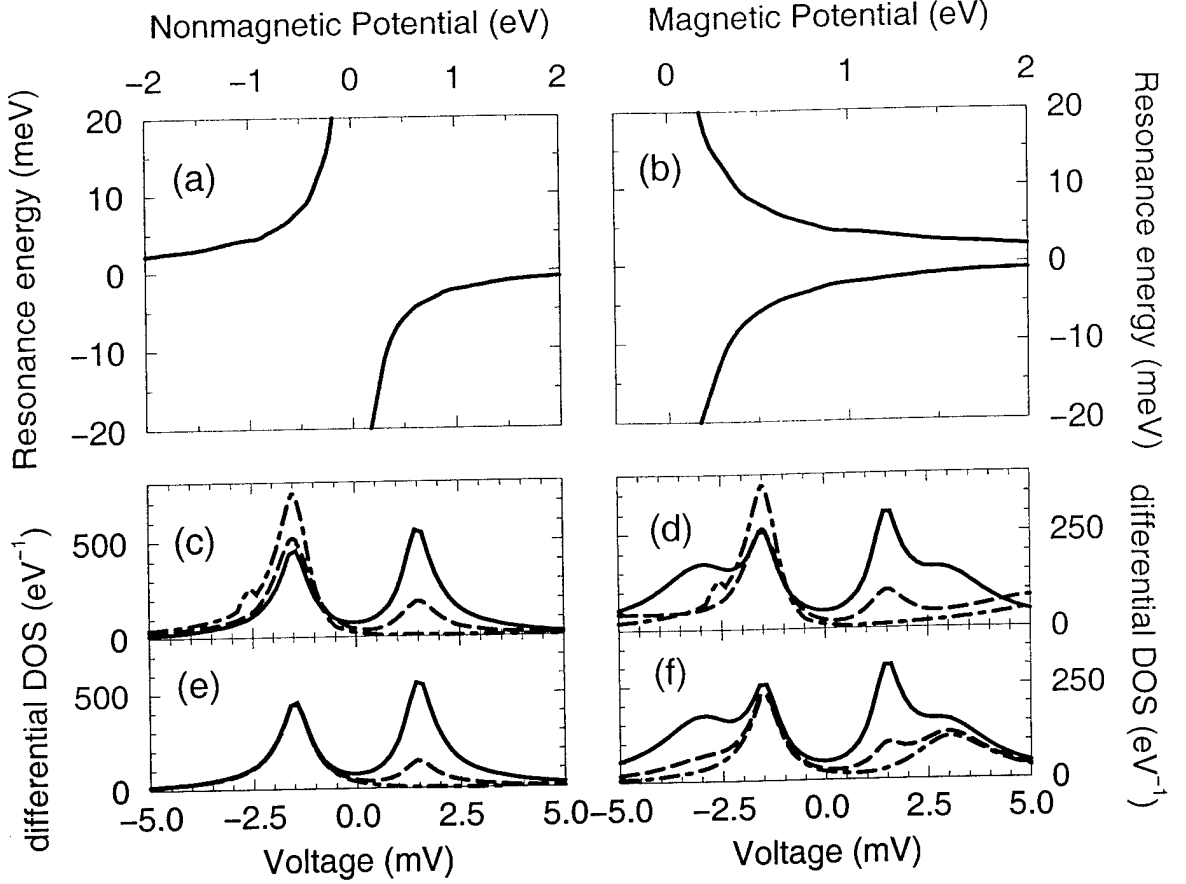[15] M. E. Flatté and D. E. Reynolds, to be published (cond-mat/9912195).

FIG. 1. Resonance energies for single-site (a) nonmagnetic and (b) magnetic impurity potentials. DOS for (c) nonmagnetic and (d) magnetic impurity potentials which produce a resonance at -1.5mV. Solid, 40 meV superconducting gap, dashed, 25 meV superconducting, 40 meV total gap, dot-dashed, 40 meV non-superconducting gap. (e) and (f), same as (c) and (d) except the dashed line corresponds to partial and the dot-dashed line to no phase coherence in the 40 meV superconducting system.
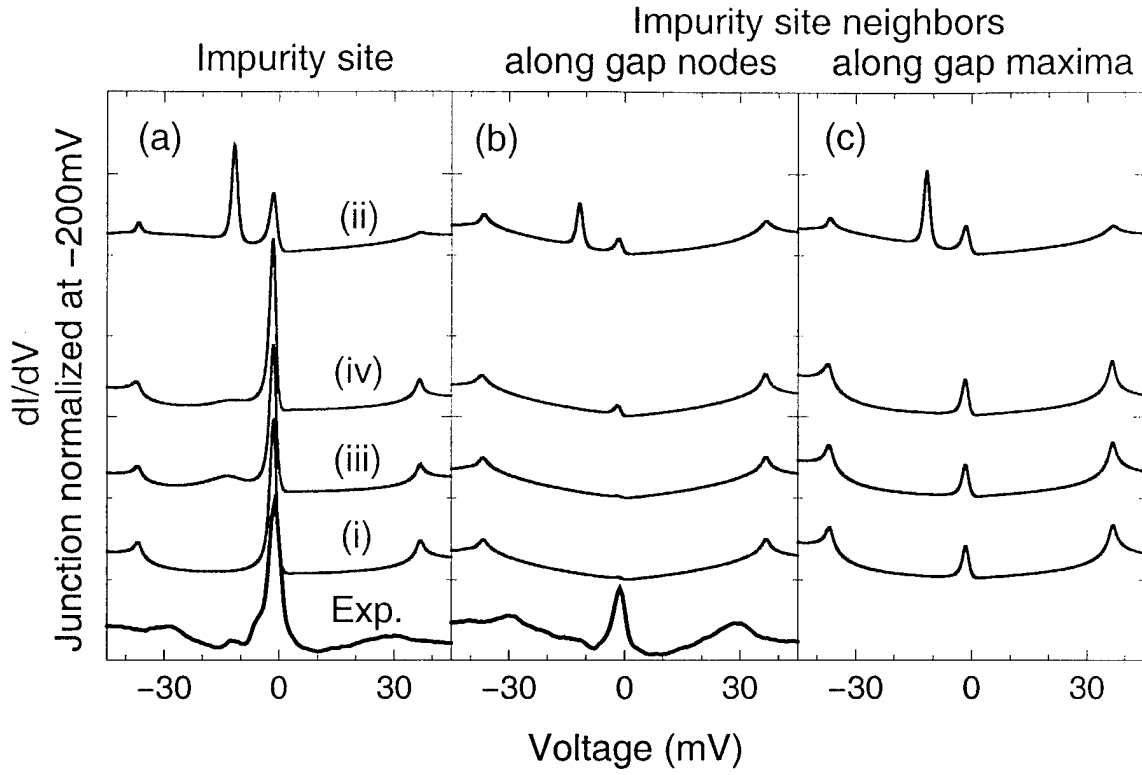
FIG. 2. dI/dV (a) on-site, (b) at the nearest-neighbor along the gap nodes, and (c) along the gap maxima, for impurity and host models i, ii, iii, and iv. Data of Ref. [5] is also shown. The order of vertical offsets (introduced for clarity) of the curves in (b) and (c) is the same as in (a).
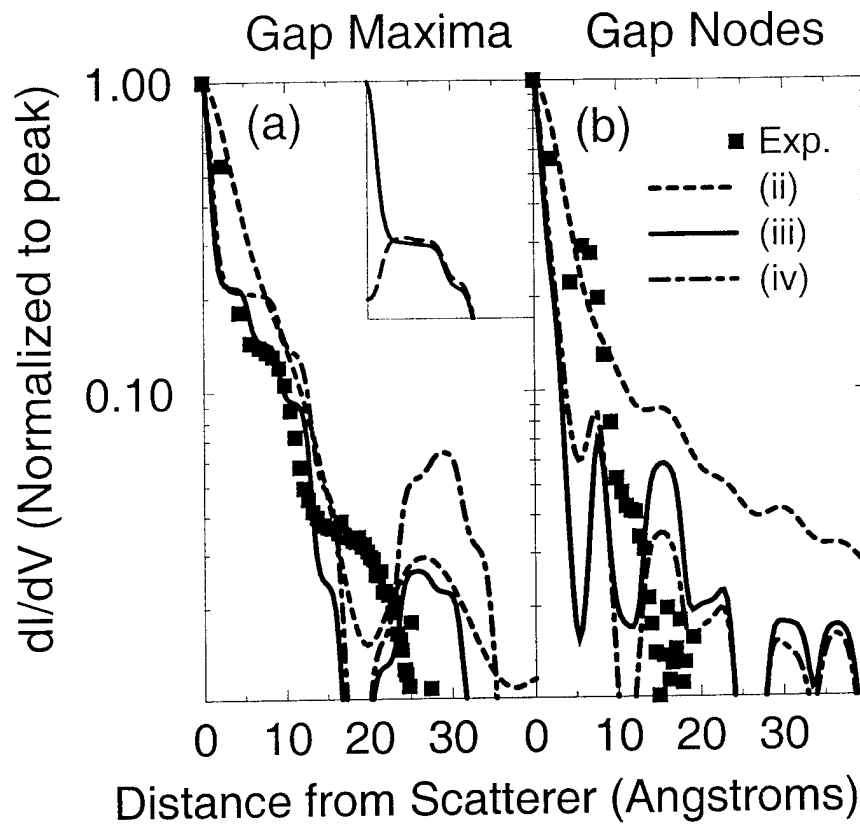
FIG. 3. dI/dV as a function of position along (a) the gap maxima and (b) the gap nodes. *ii* is dotted, *iii* is solid, and *iv* is dot-dashed. Shown in inset is the difference between dI/dV when junction normalization is (solid) and is not (dashed) taken into account.
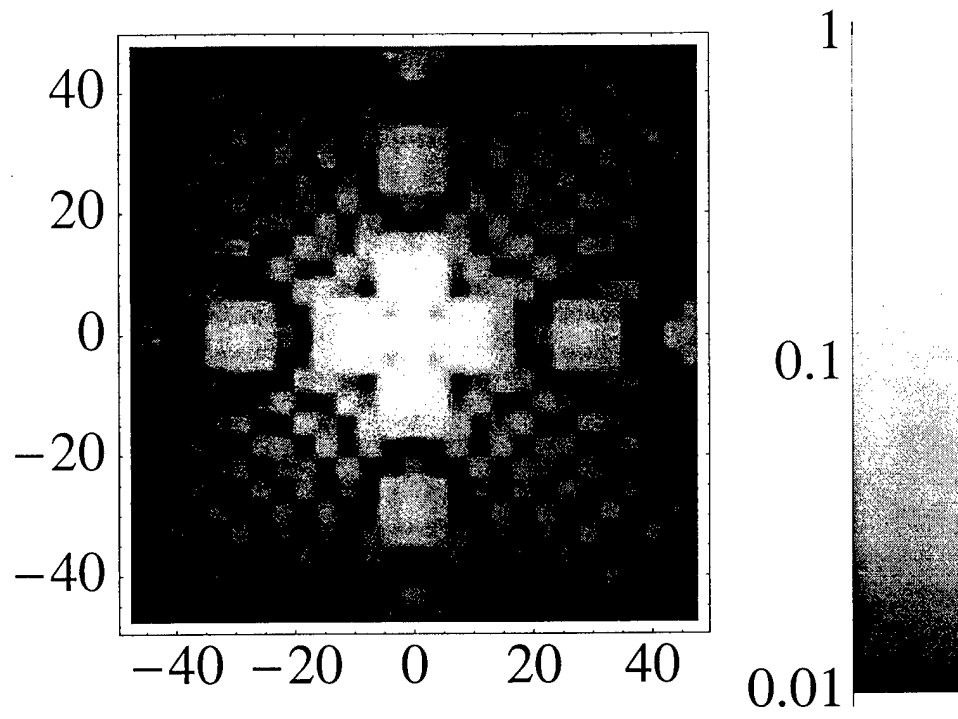
FIG. 4. Spatial structure of the dI/dV at the impurity resonance voltage (-1.5 mV) for iv. Horizontal is parallel to the gap maxima directions.

The local spectrum of a superconductor as a probe of interactions between magnetic impurities

Michael E. Flatté and David E. Reynolds

Department of Physics and Astronomy, University of Iowa, Iowa City, Iowa 52242

Abstract

Qualitative differences in the spectrum of a superconductor near magnetic impurity pairs with moments aligned parallel and antiparallel are derived. A proposal is made for a new, nonmagnetic scanning tunneling spectroscopy of magnetic impurity interactions based on these differences. Near parallel impurity pairs the mid-gap localized spin-polarized states associated with each impurity hybridize and form bonding and anti-bonding molecular states with different energies. For antiparallel impurity moments the states do not hybridize; they are degenerate.

The relative orientation of the moments of two magnetic impurities embedded nearby in a metallic nonmagnetic host will depend on the significance of several electronic correlation effects, such as direct exchange, double exchange, superexchange, and RKKY. Each of these effects produces characteristic moment orientation; the RKKY interactions can align moments either parallel or antiparallel depending on the impurity separation. Reliable experimental measurements of the moment orientation as a function of impurity separation could identify the origin of magnetism in alloys of technological significance, such as the metallic ferromagnetic semiconductor GaMnAs [1] which may eventually play a crucial role in semiconductor-based magnetoelectronics [2]. Such measurements should also clarify the interplay between metallic and magnetic behavior in layered oxides, such as the high-temperature superconductors. In this work we propose, based on theoretical calculations, a robust experimental technique for the systematic and unambiguous experimental determination of moment alignment as a function of impurity separation.

We demonstrate that in an electronic system with a gap there is a fundamental difference between the electronic states localized around parallel and antiparallel impurity moments. Around parallel impurity moments there are mid-gap molecular states (similar to bonding and antibonding states in a diatomic molecule). Around antiparallel impurity moments the states remain more atomic-like and are degenerate. This qualitative difference in the spectrum of an impurity pair provides a robust technique of determining the impurity-impurity interaction via *nonmagnetic* scanning tunneling spectroscopy (STS). The essential condition for practical application of this technique will be whether the splitting of the states around parallel impurity moments is large enough to be observed spectroscopically.

The gapped system we consider in detail is the superconductor $NbSe_2$, which is chosen for its extremely favorable surface properties for STS and for its quasi-two-dimensional electronic structure. STS has already been used to examine the localized states which form near isolated magnetic impurities on the surface of superconducting niobium [3,4]. We have

calculated the energies and spatial structure of the electronic states near impurity pairs in NbSe$_2$ essentially exactly within mean-field theory. These calculations indicate that the size of the splitting of states around parallel impurity moments in NbSe$_2$ is measurable — they are split by a sizable percentage of the energy gap even for impurity moment separations of order 30Å.

A nonmagnetic spectroscopy of magnetic impurity interactions is also plausible in a much wider range of materials. The localized spin-polarized states upon which the technique is based occur near magnetic impurities in most systems where there is a gap in the single-particle density of states at the chemical potential, whether or not the gap originates from superconductivity. Even when there is no true gap, if the density of states is substantially reduced at the chemical potential sharp resonances similar to the localized states will form (this has been predicted and recently observed for d-wave superconductors [5–7]). Resonances around parallel and antiparallel impurity pairs show similar qualitative features to localized states.

If the energy scales of moment formation and interaction are much greater than those responsible for creating the gap it is also possible to infer the impurity interaction within a material in its high-temperature metallic phase from spectroscopic measurements on the same material in a low-temperature superconducting phase. In this the STS procedure is similar to traditional "superconducting spectroscopy", [8] where the dependence on impurity concentration of the superconducting transition temperature T_c or the specific heat discontinuity at T_c is used to determine the presence and rough magnitude of a single impurity moment. However, whereas single-impurity information can often be extracted from such measurements in the dilute limit, pairwise impurity interactions are much more difficult to infer from macroscopic properties like T_c which depend on an ensemble of local configurations.

We note that the technique described here is remarkably non-invasive compared to alter-

3

nate methods. The use of a magnetic tip to probe the magnetic properties of a sample [11] may distort the natural surface orientation of moments. An alternative nonmagnetic STS technique that has been proposed, which involves a superconducting tip [12] in a Tedrow-Meservey geometry [13], requires either an external or surface-induced magnetic field to spin-split the superconducting DOS of the tip. Finally, the use of spin-polarized tunneling from a GaAs tip relies on a fixed orientation of the magnetic structure on the surface relative to that of the optically generated spin-polarized population in the tip [14].

To understand the origin of the non-degeneracy of states around parallel moments and the degeneracy of states around antiparallel moments consider a heuristic picture of the two-impurity system in an isotropic-gap superconductor. For parallel alignment of the impurity moments only quasiparticles of one spin direction (assumed to be spin up) will be attracted to the impurity pair. Any localized state will thus be spin up. If the two impurities are close their two spin-up atomic-like states will hybridize and split into molecular states just as atomic levels are split into bonding and antibonding states in a diatomic molecule. Thus there will be two non-degenerate states apparent in the spectrum. This is shown schematically in the top section of Fig. 1, where the potential for spin up quasiparticles is shown on the left (Fig. 1A) and for spin down quasiparticles is shown on the right (Fig. 1B). The potential for spin-down quasiparticles is everywhere repulsive, so no spin-down localized states will form.

The situation for antiparallel aligned spins, shown on the bottom of Fig. 1, is quite different. The effect of the second impurity on the state around the first is *repulsive* and so does not change the state energy much unless the impurities are very close. Furthermore the Hamiltonian has a new symmetry in this case: it is unchanged under the operation which both flips the quasiparticle spin and inverts space through the point midway between the two impurities. This operation changes the potential of Fig. 1C into that of Fig. 1D. Thus instead of split states we find two degenerate atomic-like states of opposite spin, localized

4

around each of the two impurities.

Detailed results for NbSe$_2$ are obtained by solving the following lattice-site mean-field Hamiltonian self-consistently:

$$H = -\sum_{\langle ij\rangle,\sigma} t_{ij} c_{i\sigma}^\dagger c_{j\sigma} + \sum_i \left[\Delta_i c_{i\uparrow}^\dagger c_{i\downarrow}^\dagger + \Delta_i^* c_{i\downarrow} c_{i\uparrow}\right] + V_{S1}(c_{1\uparrow}^\dagger c_{1\uparrow} - c_{1\downarrow}^\dagger c_{1\downarrow}) + V_{S2}(c_{2\uparrow}^\dagger c_{2\uparrow} - c_{2\downarrow}^\dagger c_{2\downarrow}),$$

(1)

where $c_{i\sigma}^\dagger$ and $c_{i\sigma}$ create and annihilate an electron at lattice site i with spin σ. The impurities reside at lattice sites 1 and 2, the t_{ij} are the hopping matrix elements and the Δ_i are the values of the superconducting order parameter. NbSe$_2$ has a triangular lattice, and the normal-state band structure can be modeled with an on-site energy of -0.1 eV and with nearest-neighbor and next-nearest-neighbor hopping matrix elements of -0.125 eV. These are determined from a tight-binding fit [9] to *ab initio* calculations of the electronic structure [10]. The superconducting pairing interaction is modeled with an on-site attractive potential which yields the experimental order parameter $\Delta = 1$ meV. The inhomogeneous order parameter Δ_i is determined self-consistently from the distorted electronic structure in the vicinity of the impurities. We consider equivalent parallel ($V_{S1} = V_{S2}$) or antiparallel ($V_{S1} = -V_{S2}$) impurity moments.

This model assumes the impurity spins behave as classical spin (see Refs. [3,4,6]). Classical spin behavior has been seen, for example, for Mn and Gd impurities on the surface of niobium [3]. The electronic structure in this model, including quasiparticle state energies and spatial structure, can be found rapidly and accurately by inverting the Gor'kov equation in a restricted real-space region including the two impurities, as described in Ref. [6]. Measurements of the spatial structure of these states and of the values of the splitting between states can serve as a sensitive test of the model of the electronic structure of this material and of the impurity potential for a given atom.

Figure 2A shows the energies of the localized states in NbSe$_2$ for parallel spins (red)

5

and antiparallel spins (black) for a sequence of impurity spacings which are multiples of the in-plane nearest-neighbor vector of the NbSe$_2$ lattice. The splitting of the bonding and antibonding states oscillates over a distance scale comparable to the Fermi wavelength of NbSe$_2$ along this direction. The splitting is proportional to the probability of a quasiparticle at one impurity propagating to the other, which is a measure of the coupling of the two atomic-like states. At large distances state energies for parallel and antiparallel moments approach the single impurity state energy, indicated on the right side of Fig. 2A. Figure 2BC shows the spatially integrated change in density of states due to the impurity pair for these impurity separations. The density of states (DOS) of a quasiparticle of energy E in a superconductor has an electron component at energy E and a hole component at energy $-E$, so a single state will produce two peaks in the DOS unless it is closer to $E = 0$ than the linewidth. That linewidth is determined by thermal broadening in the metallic probe tip, which for these plots is assumed to be 0.05 meV= 0.6K. The gap in the homogeneous DOS extends from -1 meV to 1 meV in NbSe2, so the variation in state energies is a substantial fraction of this gap. The clear distinction between parallel and antiparallel impurity moments in the DOS is only limited by the linewidth of the states.

A tunneling measurement of the DOS using a broad-area contact would yield the spectrum of an ensemble of impurity separations, hence STS (which measures the local DOS, or LDOS) is the ideal method for examining a single configuration of impurities. Before describing the distinct spatial differences in LDOS measurements between parallel and antiparallel alignments of impurity pairs we show the single impurity result in Fig. 3. The spatial structure of the electron and hole components of the LDOS are independently measurable by STS and can be quite different in detail. In this work we will show only the spatial structure of the hole component — similar gross structure is seen in the electron-like LDOS. Figure 3 shows the six-fold symmetric LDOS for NbSe$_2$ for $V_S = 200$ meV at an energy of -0.19 meV. The units are Angstroms and the nearest-neighbor spacing is 3.47Å.

The details of the spatial structure can be traced directly to the normal-state electronic structure of NbSe$_2$. [6] We note that the local hopping matrix elements and the local non-magnetic potential will differ near the impurity atoms. We find that moderate changes in these quantities do not significantly change the magnitude of the splitting of the even and odd parity states. This relative insensitivity occurs because the splitting is largely dependent on the amplitude for a quasiparticle to propagate from one impurity site to the other. Careful comparison of a measured LDOS and Fig. 3 would allow the determination of the changes in the local hopping and the nonmagnetic potential for this case.

Plots of the LDOS for two impurities in NbSe$_2$ separated by four lattice spacings (13.88Å) are shown in Fig. 4A-D. They demonstrate via their spatial structure the qualitative differences among different types of molecular states possible around an impurity pair. Figure 4A is the bonding state (energy -0.10 meV) and Fig. 4B shows the antibonding state (-0.26 meV). The impurities are at the same sites in each of Fig. 4A-D, labeled 1 and 2 in Fig. 4B. As expected from the symmetry of these states, the antibonding state has a nodal line along the mirror plane (indicated in red) between the two impurities. No such nodal line occurs in Fig. 4A — in contrast the state is enhanced along the nodes.

The nonmagnetic STS probe cannot resolve the spin direction of the electronic states around the impurities, so around antiparallel impurity moments it detects both states. The sum of the LDOS for the two atomic-like states is symmetric around the mirror plane. Figure 4C is the LDOS at the energy for the two degenerate states around antiparallel impurity spins (-0.28 meV). The states are much more diffuse than the bonding state in Fig. 4A due to the repulsive nature of one impurity. Figure 4D shows the experimentally inaccessible spin-resolved LDOS, showing the LDOS of holes with the spin direction attracted to the impurity on the left. The spin-resolved LDOS at the impurity on the left is two orders of magnitude greater than at the impurity on the right. Thus the individual localized states are quite atomic-like.

We have assumed throughout that the impurity moments are locked either parallel or antiparallel. If the alignment is intermediate between the two cases then the spectrum shows non-degenerate states split less than in the parallel case. If there is some flipping of moments between parallel and antiparallel alignment on a timescale longer than the time required for the quasiparticle states to realign with the moments then the spectrum would be a linear superposition of the antiparallel and parallel spectra. If this is an activated process, this energy of activation of moment flipping could be easily distinguished by examining the temperature dependence of the spectrum.

This work describes a robust technique for determining the alignment of two impurity moments in a gapped system. The details of the expected results around magnetic impurities in the quasi-two-dimensional superconductor $NbSe_2$ have been calculated. Energies and spatial structure of bonding and antibonding states around parallel moments, and of localized atomic-like states around antiparallel moments, indicate the two cases should be distinguishable with nonmagnetic scanning tunneling spectroscopy. This technique should be broadly applicable to a wide range of correlated electronic systems.

REFERENCES

[1] B. Beschoten, *et al.*, unpublished.

[2] H. Ohno, Science **281**, 951 (1998).

[3] A. Yazdani, B. A. Jones, C. P. Lutz, M. F. Crommie, and D. M. Eigler, Science **275**, 1767 (1997).

[4] H. Shiba, Prog. Theor. Phys. **40**, 435 (1968).

[5] M. I. Salkola, A. V. Balatsky, and D. J. Scalapino, Phys. Rev. Lett. **77**, 184 (1996).

[6] M. E. Flatté and J. M. Byers, in *Solid State Physics Vol. 52*, ed. H. Ehrenreich and F. Spaepen, Academic Press, New York, 1999.

[7] E. W. Hudson, *et al.*, Science **285**, 88 (1999); A. Yazdani, C. M. Howald, C. P. Lutz, A. Kapitulnik, and D. M. Eigler, Phys. Rev. Lett., **83**, 176 (1999).

[8] M. B. Maple, in *Moment Formation in Solids*, ed. W. J. L. Buyers, Plenum, New York (1984), p. 1.

[9] W. Sacks, D. Roditchev, and J. Klein, Phys. Rev. B **57**, 13118 (1998).

[10] A. Kikuchi and M. Tsukada, Surf. Sci. **326**, 195 (1995).

[11] M. Bode, M. Getzlaff, and R. Wiesendanger, Phys. Rev. Lett. **81**, 4256 (1998).

[12] S. H. Pan, E. W. Hudson, and J. C. Davis, Appl. Phys. Lett. **73**, 2992 (1998).

[13] R. Meservey, Phys. Scr. **38**, 272 (1988).

[14] S. F. Alvarado and P. Renaud, Phys. Rev. Lett. **68**, 1387 (1992); S. F. Alvarado, Phys. Rev. Lett. **75**, 513 (1995).
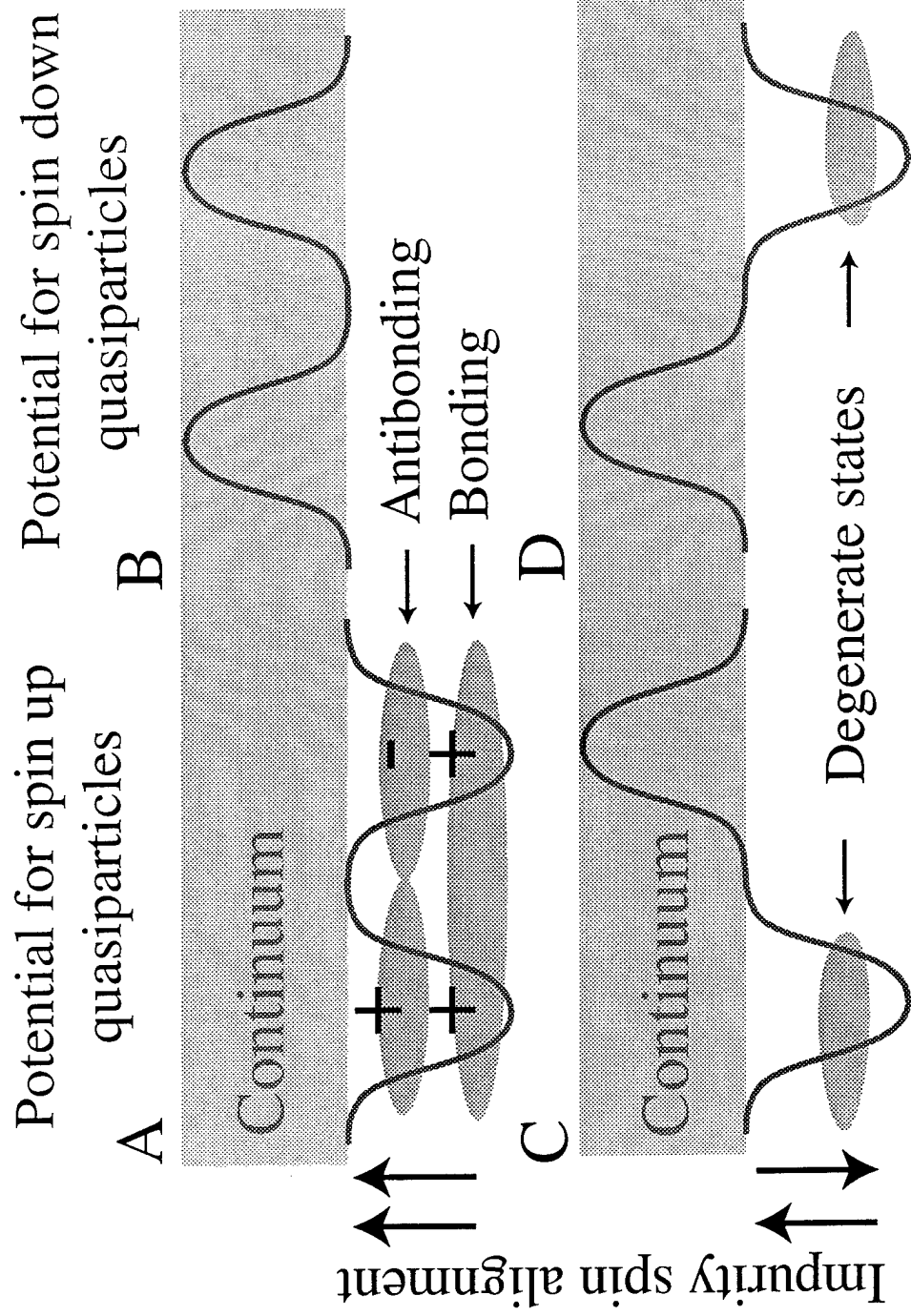
FIGURES

FIG. 1. (color) Schematic of the potential for spin-up (left side, (A) and (C)) and spin-down (right-side, (B) and (D)) quasiparticles in the presence of parallel impurity spins (top row, (A) and (B)) and antiparallel impurity spins (bottom row (C) and (D)). For parallel impurity spins there are two localized states of spin-up quasiparticles which differ in energy, similar to the bonding and antibonding states of a diatomic molecule. There are no localized states of spin-down quasiparticles. For antiparallel impurity spins there is one spin-down quasiparticle localized state, as well as one of spin up, and the two are degenerate.
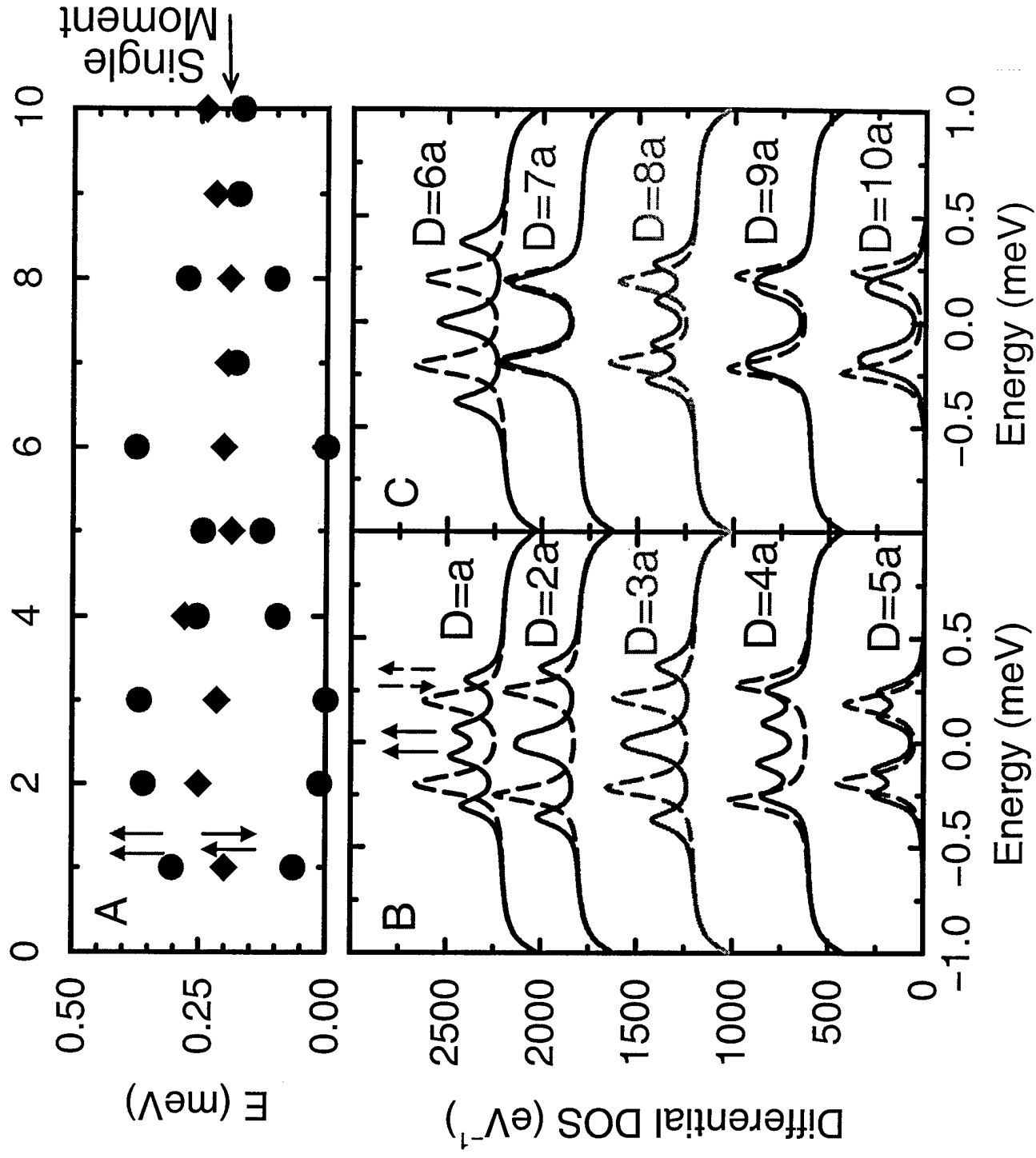
FIG. 2. (color) (A) Energies of localized states as a function of impurity separation near parallel impurity spins (red) and antiparallel impurity spins (black). Energy is in meV and impurity separation in nearest-neighbor in-plane lattice constants (3.47Å). (B) Differential density of states (DOS) for parallel impurity pairs (solid lines) and antiparallel impurity pairs (dashed lines) for impurity separations from one to five lattice spacings. (C) Same as (B), except for six to ten lattice spacings.
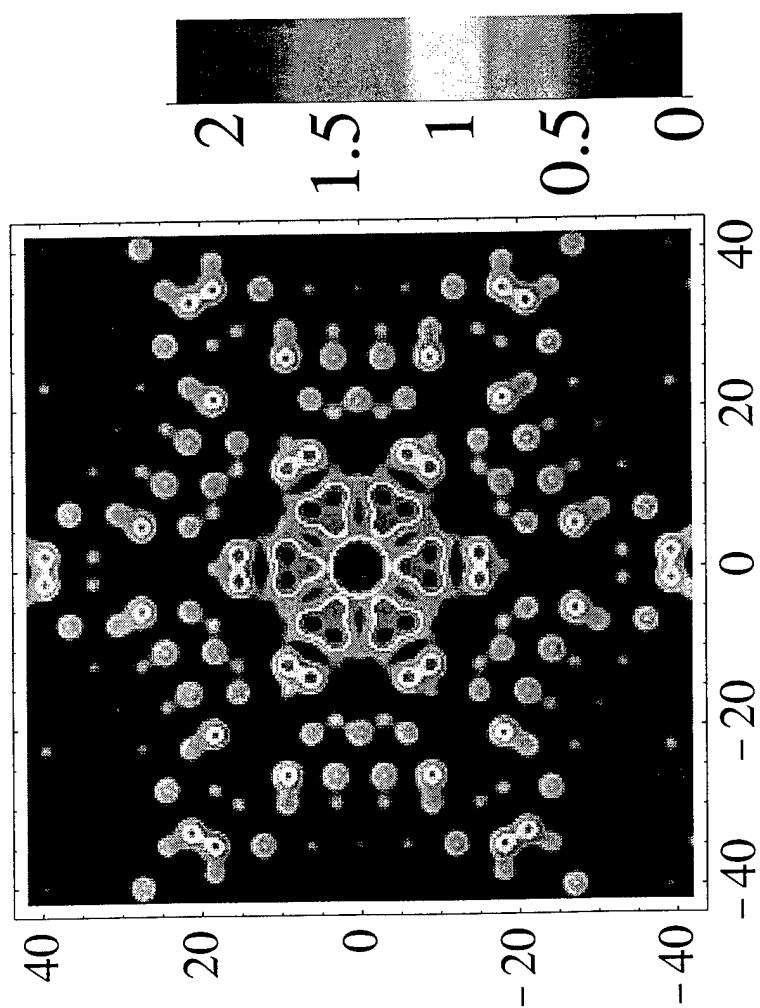
FIG. 3. (color) Spatial structure of the hole-like local density of states (LDOS) around a single impurity in the surface layer of $NbSe_2$. Nearest-neighbor in-plane separation on the triangular lattice is 3.47Å. The units of the color scale are eV^{-1}.

FIG. 4. (color) LDOS around a parallel impurity pair at (A) the energy corresponding to the bonding state (−0.10 meV), and (B) the energy corresponding to the antibonding state (−0.26 meV). The impurities are at the same sites in each of (A-D), labeled 1 and 2 in (B). The mirror plane between the impurities is indicated by the red line in (B); there is no LDOS for the antibonding state in (B) along this plane, while there is for the bonding state (A). (C) LDOS around an antiparallel impurity pair at the energy of localized states (−0.28 meV). (D) spin-resolved LDOS at the same energy as (C) showing the predominance of LDOS around the impurity on the left. The units of the color scale are eV^{-1}.
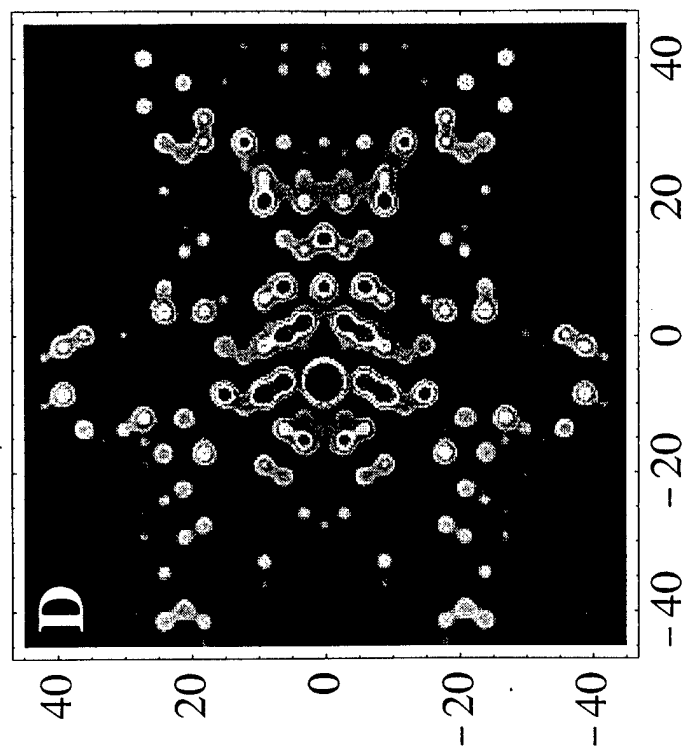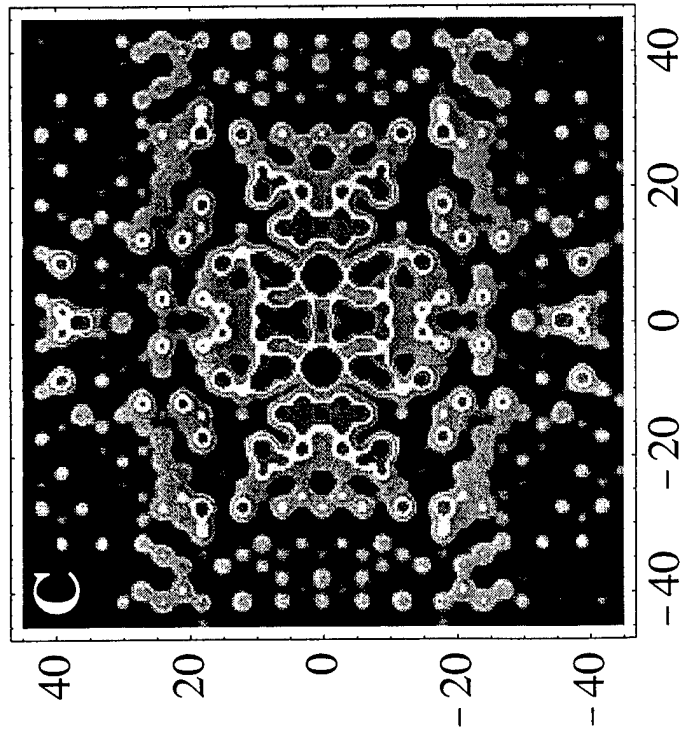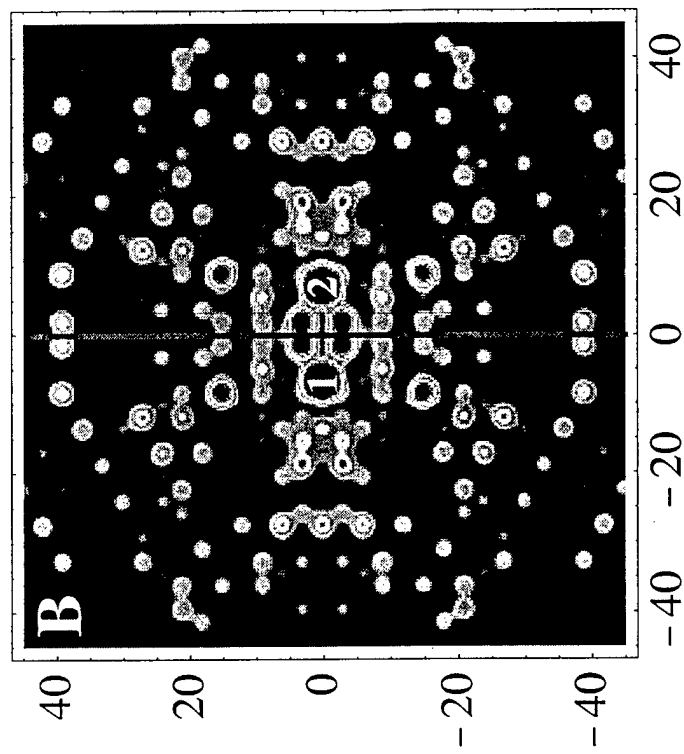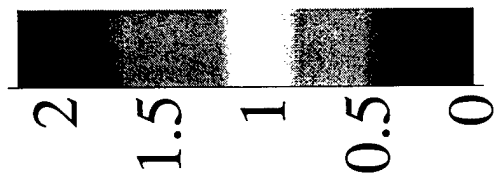
Potential for spin up quasiparticles

Potential for spin down quasiparticles

A

B

C

D

Continuum

Continuum

Antibonding

Bonding

Degenerate states

Impurity spin alignment

A (top panel, rotated)

Single Moment ↓

Separation (lattice spacings a=3.47 Angstroms)

E (meV)

B / **C** (lower panels)

Differential DOS (eV^{-1})

Energy (meV)

D=a, D=2a, D=3a, D=4a, D=5a

D=6a, D=7a, D=8a, D=9a, D=10a
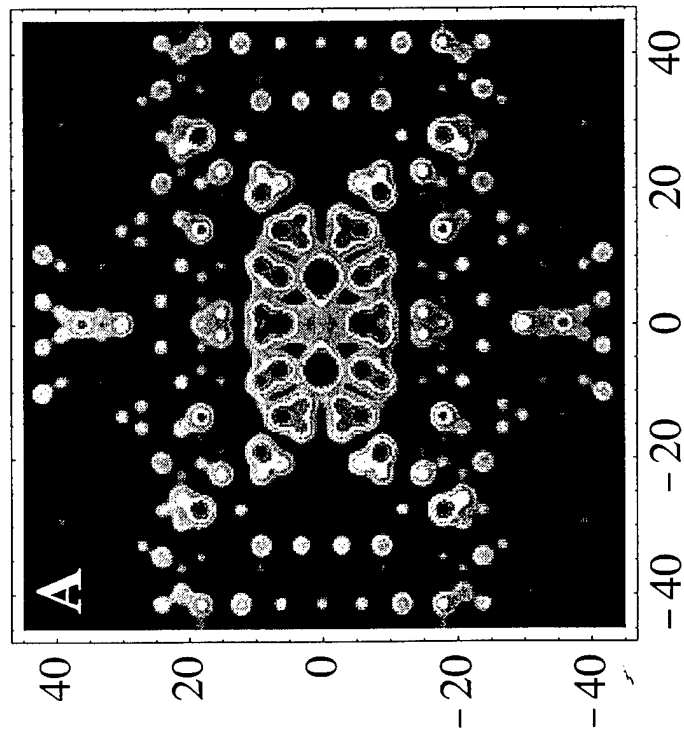
REPORT DOCUMENTATION PAGE

Public reporting burden for this collection of information is estimated to average 1 hour per response, including the time for reviewing instructions, searching existing data sources, gathering and maintaining the data needed, and completing and reviewing the collection of information. Send comments regarding this burden estimate to any other aspect of this collection of information, including suggestions for reducing this burden, to Washington Headquarters Services, Directorate for Information Operations and Reports, 1215 Jefferson Davis Highway. Suite 1204, Arlington. VA 22202-4302. and to the Office of Management and Budget, paperwork Reduction Project (0704-0188). Washington, DC 20503.

1. AGENCY USE ONLY (Leave blank)	2. REPORT DATE March 1,2000	3. REPORT TYPE AND DATES COVERED Performance (5 March 99– 4 March00)

4. TITLE AND SUBTITLE
The Effects of Impurities on Junction Behavior in High-Temperature Superconductors

5. FUNDING NUMBERS
N00014-99-0313

6. AUTHOR(S)
Michael E. Flatté

7. PERFORMING ORGANIZATION NAME(S) AND ADDRESS(ES)
University of Iowa
Iowa City, IA 52242

8. PERFORMING ORGANIZATION REPORT NUMBER

9. SPONSORING /MONITORING AGENCY NAME(S) AND ADDRESS(ES)
Office of Naval Research
Ballston Centre Tower One
800 North Quincy Street
Arlington VA 22217-5660

10. SPONSORING /MONITORING AGENCY REPORT NUMBER

11. SUPPLEMENTARY NOTES

12a. DISTRIBUTION/AVAILABILITY STATEMENT

APPROVED FOR PUBLIC RELEASE

12b. DISTRIBUTION CODE

13. ABSTRACT *(Maximum 200 words)*

This is a report on the progress in theoretical calculations of scanning tunneling microscopy spectra near impurities in superconductors. Calculations have been performed for Zn and Ni impurities in BSCCO, and compared with recent scanning tunneling microscopy spectra near those impurities. Good quantitative agreement has been found. The Zn atom appears to locally destroy superconductivity. New experiments involving two Ni atoms and a Ni and Zn atom have been proposed to clarify the range of this effect from Zn, and also to observe the spin-spin correlation function in the superconducting state.

14. SUBJECT TERMS
Superconductivity, magnetic impurities, scanning tunneling microscopy, BSCCO, Zn impurities, Ni impurities

15. NUMBER OF PAGES
22

16. PRICE CODE

17. SECURITY CLASSIFICATION OF REPORT	18. SECURITY CLASSIFICATION OF THIS PAGE	19. SECURITY CLASSIFICATION OF ABSTRACT	20. LIMITATION OF ABSTRACT

NSN 7540-01-280-5500